Spin-Wave Dispersion in Orbitally Ordered $La_{1/2}Sr_{3/2}MnO_4$

D. Senff,[1] F. Krüger,[2,3] S. Scheidl,[2] M. Benomar,[1] Y. Sidis,[4] F. Demmel,[5] and M. Braden[1,*]

[1]*II. Physikalisches Institut, Universität zu Köln, Zülpicher Strasse 77, D-50937 Köln, Germany*
[2]*Institut für Theoretische Physik, Universität zu Köln, Zülpicher Strasse 77, D-50937 Köln, Germany*
[3]*Instituut-Lorentz, Universiteit Leiden, P.O. Box 9506, 2300 RA Leiden, The Netherlands*
[4]*Laboratoire Léon Brillouin, C.E.A./C.N.R.S., F-91191 Gif-sur-Yvette Cedex, France*
[5]*Institut Laue-Langevin, Boîte Postale 156, 38042 Grenoble Cedex 9, France*

(Received 13 December 2005; published 26 June 2006)

The magnon dispersion in the charge, orbital, and spin ordered phase in $La_{1/2}Sr_{3/2}MnO_4$ has been studied by means of inelastic neutron scattering. We find excellent agreement with a magnetic interaction model based on the CE-type superstructure. The magnetic excitations are dominated by ferromagnetic exchange parameters revealing a nearly one-dimensional character at high energies. The strong ferromagnetic interaction in the charge or orbital ordered phase appears to be essential for the capability of manganites to switch between metallic and insulating phases.

DOI: 10.1103/PhysRevLett.96.257201 PACS numbers: 75.30.Ds, 71.10.−w, 75.47.Lx, 75.50.Ee

Colossal magnetoresistivity in the manganites is only partially explained by the Zener double-exchange mechanism; the larger part of it appears to arise from the competition of two states: the metallic ferromagnetically ordered state on the one side and the insulating one with a cooperative ordering of charges, orbitals, and spins (COS) on the other side [1,2]. The insulator to metal transition consists in switching from a phase with long- or short-range COS correlations into the metallic state where spins are aligned either by a magnetic field or by spontaneous magnetic order. Such an interpretation is strongly supported by studies of the diffuse scattering: The decrease in electronic resistivity is found to scale with the suppression of COS correlations as a function of either temperature [3,4] or magnetic field [5].

In spite of its eminent relevance for colossal magnetoresistivity, the exact nature of the COS states in the manganites has not yet been fully established. The combined COS ordering was first studied in the pioneering work by Wollan and Koehler [6] and by Goodenough [7] proposing the so-called CE-type arrangement, which is illustrated in Fig. 1(a). For half-doping, i.e., equal amounts of Mn^{3+} and Mn^{4+}, there is a checkerboard arrangement of different charges. In addition, the e_g orbitals at the Mn^{3+} sites form zigzag chains. The CE-type charge and orbital arrangement will yield a ferromagnetic interaction in the zigzag chains and an antiferromagnetic one in between. In the recent literature, there is evidence both for [8,9] and against [10] this CE-type picture of the COS state near half-doping. The quantitative structural analysis excludes a full ordering of charges and orbitals [8,9] which would induce stronger structural distortions. Recently, a qualitatively different scheme was proposed for $Pr_{0.6}Ca_{0.4}MnO_3$ where charges do not order on the metal sites but on the Mn-O-Mn bonds forming Zener polarons [10]. Whether this Zener-polaron picture is applicable for all manganites or whether it is relevant at all is still under debate [11].

The magnetic excitations in the ferromagnetic metallic manganites have been studied in many different compositions [12–15]; for a recent summary, see Ref. [15]. In view of the large amount of data on the ferromagnetic phases, it may astonish the reader that there is still no detailed study

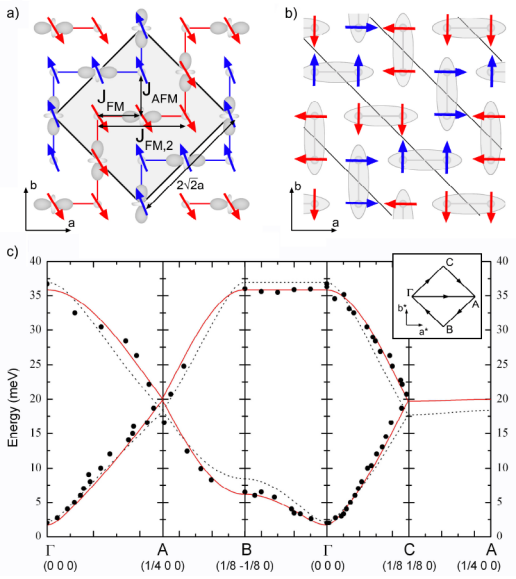

FIG. 1 (color online). (a) Schematic representation of the CE-type ordering in the *ab* plane of half-doped manganites with the three magnetic interaction parameters described in the text. Notice that the FM zigzag chains run along the [110] direction. (b) Schematic arrangement in the Zener-polaron picture [31]. (c) Dispersion of the magnetic excitations in $La_{1/2}Sr_{3/2}MnO_4$ in a direction parallel to [100] (Γ to A), perpendicular to the chains (Γ to B), and parallel to the chains (Γ to C). The solid and dashed lines give the spin-wave dispersion calculated with two parameter sets; see text. Inset: Sketch of the magnetic Brillouin zone, displaying the high symmetry points $\Gamma = (0, 0, 0)$, $A = (1/4, 0, 0)$, $B = (1/8, -1/8, 0)$, $C = (1/8, 1/8, 0)$, and the path of the calculated dispersion.

on magnetic excitations in antiferromagnetic COS states. Besides the intrinsic complexity of the CE-type magnetic ordering, such a study is severely hampered by the twinning of the manganite crystals in the perovskite phases. We, therefore, have chosen the layered material $La_{1/2}Sr_{3/2}MnO_4$ to study the magnon dispersion in the COS state. We obtain the full dispersion of the two magnon branches with lowest energies which may be satisfactorily described in the CE-type model.

The structural, electronic, and magnetic phase diagram of $La_{1+x}Sr_{1-x}MnO_4$ has been elaborated in Refs. [16–18]. For $x = 0$, $LaSrMnO_4$, all Mn are threevalent with occupation of the $(3z^2 - r^2)$ e_g orbitals and spins ordered antiferromagnetically. The half-doped compound $La_{1/2}Sr_{3/2}MnO_4$ exhibits cooperative COS ordering, which has been studied by various techniques [19–23]. Compared to most perovskite manganites at half-doping, the COS state in $La_{1/2}Sr_{3/2}MnO_4$ appears to be rather stable; only in very high magnetic fields of the order of 30 T is the COS state suppressed and colossal magnetoresistivity observed [24], but good metallic properties are never achieved in the single-layered manganites neither by field nor by doping.

The single crystal used in this study was grown by the floating zone technique as described in Ref. [25] (volume 0.6 cm^3, space group $I4/mmm$, $a = 3.86$ Å and $c = 12.42$ Å at room temperature). Upon cooling, we observe the sequence of structural and magnetic ordering following the appearance of the respective superstructure reflections in neutron diffraction experiments. Orbital and charge ordering within the CE-type picture is related with superstructure reflections displaced from reciprocal lattice vectors by $\mathbf{q} = (\pm\frac{1}{4}, \pm\frac{1}{4}, 0)$ and by $(\pm\frac{1}{2}, \pm\frac{1}{2}, 0)$, respectively (we use reduced lattice units of $\frac{2\pi}{a}$ with respect to the $I4/mmm$ cell). The onset of charge or orbital ordering is observed at $T_{CO/OO} = 230$ K in agreement with Refs. [19,21]. In addition, below $T_N = 110$ K antiferromagnetic ordering is evidenced through magnetic reflections [19]; magnetic ordering, however, is not fully three-dimensional. For the determination of the magnon dispersion, the lack of correlations along the c direction is irrelevant, as the magnetic exchange parameters are negligible along this direction. In the following, we discuss only the layered magnetic ordering.

Let us illustrate the different propagation vectors with the aid of the scheme given in Fig. 1(a). With the orbital ordering, the nuclear lattice becomes orthorhombic with lattice constants of $\sqrt{2}a$ along $[1, \bar{1}, 0]$ and $2\sqrt{2}a$ along $[1, 1, 0]$. Note that the zigzag chains run along the $[1, 1, 0]$ direction. Orbital ordering is related only to superstructure reflections with $\mathbf{q} = \pm(\frac{1}{4}, \frac{1}{4}, 0)$. Considering only the Mn^{3+} sites, the magnetic lattice is orthorhombic, too, and of the same size as the structural one but rotated by 90°, $2\sqrt{2}a$ along $[1, \bar{1}, 0]$ and $\sqrt{2}a$ along $[1, 1, 0]$. The Mn^{3+} spins contribute to magnetic superstructure reflections with $\mathbf{q} = \pm(\frac{1}{4}, -\frac{1}{4}, 0)$; for example, there is a contribution at $(0.25, 0.75, 0) = (0.25, -0.25, 0)$ but none at $(0.25, 0.25, 0)$. The Mn^{4+} spins do not contribute to either of these but to positions with $\mathbf{q} = \pm(0, 0.5, 0)$ or $\mathbf{q} = \pm(0.5, 0, 0)$, where the Mn^{3+} spins do not contribute. The full magnetic cell has to be described in a pseudoquadratic lattice with constants $2\sqrt{2}a$ along $[1, \bar{1}, 0]$ and $[1, 1, 0]$, as shown in Fig. 1(a). Because of the twinning in the orthorhombic COS phase, the arrangement in Fig. 1(a) (orientation I) is superposed by the same rotated by 90° (orientation II) in a sample crystal. Both twin orientations contribute equally in our sample, but we will always refer to orientation I for the analysis.

Neutron scattering experiments were performed on the triple-axis spectrometers $4F$ and $1T$ at the Orphée reactor in Saclay, France, and on $IN3$ at the Institut Laue Langevin in Grenoble, France. The sample was mounted with the [001] direction perpendicular to the scattering plane and cooled to $T = 15$ K. Monochromatic neutrons were selected using Bragg scattering from the (002) reflection of pyrolytic graphite (PG) or—at higher incident energies—the (111) reflection of copper. The final energies were, in most cases, fixed to 14.7 meV to suppress higher order contaminations with the aid of a PG filter.

At the antiferromagnetic zone center, we find a gap in the magnetic excitation spectrum and a small energy splitting of the lowest excitation. The degeneracy of the two transverse magnons appears to be lifted due to complex magnetic anisotropy terms [26]. Already for $q > 3.9 \times 10^{-3}$ Å^{-1} away from the zone center, no splitting in the magnon frequencies is resolved anymore. In spite of the twinning of the crystal in the COS phase, we are able to separate the magnon branches parallel and perpendicular to the zigzag chains, as only one twin orientation contributes to a quarter-indexed magnetic superstructure reflection. When going from the antiferromagnetic zone center $(0.75, -0.75, 0)$ along the $[1, 1, 0]$ direction, one determines the spin-wave dispersion parallel to the zigzag chains [see Fig. 2(e)], and, when going along the $[1, \bar{1}, 0]$ direction, one measures the dispersion perpendicular to the chains. This behavior is corroborated by the structure-factor calculations presented in Fig. 3 as discussed below. The raw-data scans shown in Fig. 2 unambiguously demonstrate that the dispersion along the zigzag chains is much steeper than perpendicular to them. The magnetic structure has to be considered as a weak antiferromagnetic coupling of strongly coupled ferromagnetic zigzag chains. The obtained magnon dispersion is presented in Fig. 1(c). The branch propagating along the chains, path $\mathbf{\Gamma} - \mathbf{C}$, is much steeper than the branch propagating perpendicular to it, path $\mathbf{\Gamma} - \mathbf{B}$. At the magnetic zone boundaries $\mathbf{C}$ and $\mathbf{B}$, we find magnon energies of 19 and 6.5 meV, respectively. At the point $\mathbf{C}$ where $\mathbf{q}$ is parallel to the chains, the end point of the acoustic branch coincides with that of the lowest optic branch, whereas there is a large gap between these

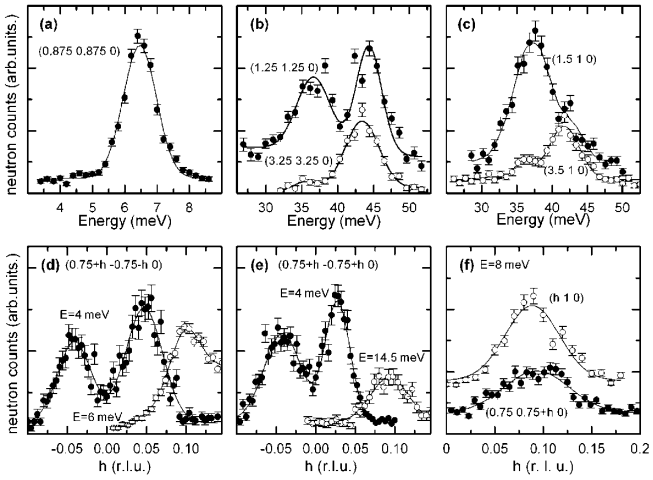

FIG. 2. Raw-data scans to determine the magnon dispersion in $La_{1/2}Sr_{3/2}MnO_4$; symbols denote data and lines fits with Gaussians. (a)–(c) Constant $\mathbf{Q}$ scans at the antiferromagnetic zone center and zone boundaries. (b) and (c) were measured with $E_f = 7.37$ meV and using the copper monochromator; the different $\mathbf{Q}$ dependence separates magnetic from phononic scattering in (b) and (c). (d)–(f) Constant-energy scans for different energies across $(0.75, -0.75, 0)$ in the $[1, \bar{1}, 0]$ direction, i.e., perpendicular to the zigzag chains (d), and in the $[1, 1, 0]$ direction, i.e., parallel to the zigzag chains (e). The scan is aiming at the dispersion along the $[0, 1, 0]$ direction, path $\mathbf{\Gamma} - \mathbf{A}$ (f).

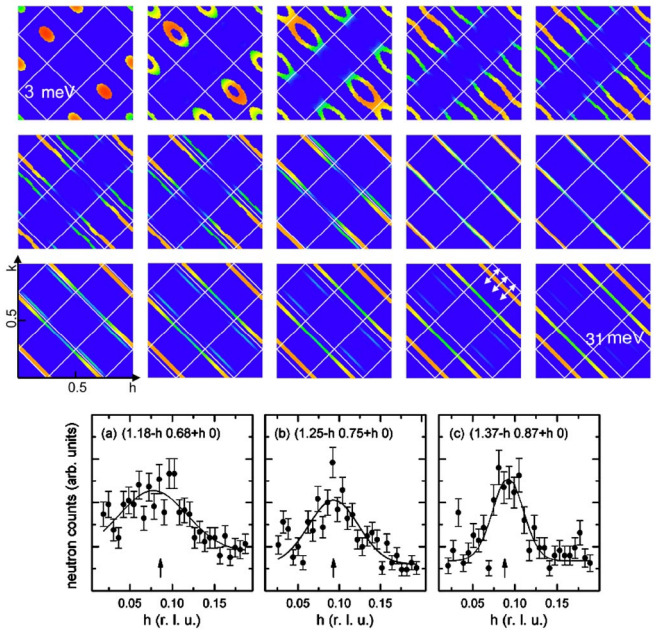

FIG. 3 (color online). Upper panel: Constant-energy cuts through the calculated spin-wave structure factor $S(\mathbf{Q}, \omega)$ with a constant-energy resolution of 2 meV within each plot and with energy steps of 2 meV between adjacent plots, showing the dispersion and scattering distribution of the lowest magnon bands. Lower panel: Constant-energy scans along the direction indicated by arrows in the 29 meV cut (above) to experimentally verify the one-dimensional character of the high energy magnetic scattering. The arrows indicate the expected positions of the magnon.

branches along the path $\mathbf{\Gamma} - \mathbf{B}$. The magnon branch along the [100] direction, path $\mathbf{\Gamma} - \mathbf{A}$ at 45° to the chains, exhibits an intermediate dispersion. Finally, all zone-boundary modes connect when passing along the zone-boundary paths $\mathbf{A} - \mathbf{B}$ and $\mathbf{A} - \mathbf{C}$.

We have performed measurements around the quarter-integer-indexed magnetic zone centers as well as around half-integer-indexed ones. As explained above, in elastic scans at these $\mathbf{Q}$ values, one strictly measures the scattering contribution of the Mn^{3+} and that of the Mn^{4+} sites, respectively. This separation should hold for inelastic scattering at rather low energies as well. Around these $\mathbf{Q}$ values, we find exactly the same dispersion, as is expected for collective magnons. At finite energies, there is also a significant structure factor around the integer-indexed $\mathbf{Q}$ values, like $(1, 0, 0)$; again, the dispersion of the modes fully agrees with the other zones. The dispersion shown in Fig. 1 was obtained finally by combining many scans in different magnetic zones. At energies significantly above the saturation of the acoustic magnon branch perpendicular to the zigzag chains, i.e., 6.5 meV, the magnetic interaction perpendicular to the chains does not play any role anymore and the magnon dispersion exhibits a one-dimensional character.

The spin-wave dispersion has been calculated using the Holstein-Primakoff transformation with a simple spin-only Hamiltonian illustrated in Fig. 1(a) (in the sums, each pair appears only once):

$$\mathcal{H} = -\sum_{(Mn^{3+},Mn^{4+})_{||}} J_{FM}\mathbf{S_i}\cdot\mathbf{S_j} + \sum_{(Mn^{3+},Mn^{4+})_{\perp}} J_{AFM}\mathbf{S_i}\cdot\mathbf{S_j} - \sum_{(Mn^{4+},Mn^{4+})_{nnn||}} J_{FM,2}\mathbf{S_i}\cdot\mathbf{S_j} - \sum_{Mn}\Lambda S_z^2.$$

Details of the calculation can be found in related work on spin excitations in stripe phases [27]. The Mn^{3+} and Mn^{4+} spins were fixed to the values of $S = 2$ and $S = 1.5$, respectively. Taking into account only the two nearest-neighbor interactions for $Mn^{3+} - Mn^{4+}$-spin interactions for pairs within and in between the zigzag chains, J_{FM} and J_{AFM}, one obtains a good description of the measured dispersion denoted in Fig. 1(c) by dashed lines. However, there remain significant discrepancies; it is impossible to simultaneously describe the large initial slope of the spin-wave dispersion along the chains and the relatively lower zone-boundary frequencies. This behavior implies the relevance of an additional longer-distance interaction parameter acting along the ferromagnetic chains. Indeed, a fully satisfactory description is obtained by including a ferromagnetic interaction for $Mn^{4+} - Mn^{4+}$-spin pairs connected through a Mn^{3+} within a zigzag chain; see the solid lines in Fig. 1(c). We determine the parameters:

$J_{FM} = 9.98$ meV, $J_{AFM} = 1.83$ meV, $J_{FM,2} = 3.69$ meV and an anisotropy term of $\Lambda = 0.05$ meV. The magnon dispersion can be described nearly as well when considering a ferromagnetic coupling between two Mn^{3+} sites along the zigzag chain, but this parameter appears less physical. This model predicts the existence of rather flat optical branches around 75 meV, which, however, could not be observed so far due to the high phonon signal at these energies. Figure 3 presents the calculated magnon scattering intensities in the form of constant-energy cuts. One can see how the anisotropic spin-wave cones develop around the magnetic Bragg peaks with a finite structure factor. At intermediate energies, also those magnetic Brillouin zones contribute where there is no elastic scattering. Figure 3 further illustrates that, well above the maximum of the acoustic magnon perpendicular to the zigzag chains, the system looks like a magnetically one-dimensional system as the magnons disperse only along the zigzag chains. The one-dimensional character was verified by special constant-energy scans; see Fig. 3. The dominant ferromagnetic coupling is furthermore seen in experiments upon heating across $T_{CO/OO}$. The diffuse magnetic scattering as well as the magnetic fluctuations turn ferromagnetic in character at high temperatures [26].

The ferromagnetic interactions in the COS phase of $La_{1/2}Sr_{3/2}MnO_4$ are remarkably large, whereas the antiferromagnetic coupling is small probably due to competing effects. J_{FM} is about a factor of 5 larger than the ferromagnetic coupling in $LaMnO_3$ [28] acting on two Mn^{3+} sites with an antiferroorbital coupling. J_{FM} is also significantly larger than the ferromagnetic interaction in the metallic ferromagnetic phases with the highest Curie temperatures [12,13]. Furukawa has studied how the double-exchange model in the metallic manganite phases maps to a Heisenberg-model description: With increasing electron localization, the spin-spin interactions become more short-range [29]. The strong ferromagnetic interaction in the zigzag chains being not restricted to the nearest neighbors indicates that electrons are not fully localized in the COS phase as well. The large and nonlocal ferromagnetic interactions in the zigzag chains yield considerable resemblance between the COS and the metallic phases. This resemblance might be essential to understand the capability of manganites to switch between the metallic ferromagnetic and the insulating COS phases. An explanation why the zigzag chains nevertheless are insulating has been given in Ref. [30].

In contrast with the excellent magnon-dispersion modeling presented above, there is no straightforward description of the observed dispersion within the Zener-polaron model. Obviously, there is a dominant ferromagnetic coupling within the Zener dimer, but the interdimer couplings are less clear. As may be seen in Fig. 1(b), the dimers are stacked in a herringbone pattern, and only the interdimer interaction along this stacking should be sizable and nonfrustrated. Efremov *et al.* [31] have proposed a noncollinear magnetic ordering [see Fig. 1(b)] different from the structure presented in the initial work [10]. This arrangement may correctly describe the diffraction signal, but it yields a spin-wave anisotropy—there is dispersion only along the dimer stacks—just opposite to our experimental result. This failure and the excellent spin-wave description obtained within the CE-type model give strong support for the latter in $La_{1/2}Sr_{3/2}MnO_4$.

Work at Universität zu Köln was supported by the Deutsche Forschungsgemeinschaft through the Sonderforschungsbereich 608. We thank L. P. Regnault and D. Khomskii for stimulating discussions.

*Electronic address: braden@ph2.uni-koeln.de

[1] Y. Tokura and N. Nagaosa, Science **288**, 462 (2000).
[2] Y. Motome *et al.*, Phys. Rev. Lett. **91**, 167204 (2003).
[3] C. P. Adams *et al.*, Phys. Rev. Lett. **85**, 3954 (2000).
[4] S. Shimomura *et al.*, Phys. Rev. Lett. **83**, 4389 (1999).
[5] F. M. Woodward *et al.*, Phys. Rev. B **70**, 174433 (2004).
[6] E. O. Wollan and W. C. Koehler, Phys. Rev. **100**, 545 (1955).
[7] J. B. Goodenough, Phys. Rev. **100**, 564 (1955).
[8] P. G. Radaelli *et al.*, Phys. Rev. B **55**, 3015 (1997).
[9] Z. Jirak *et al.*, J. Magn. Magn. Mater. **53**, 153 (1985).
[10] A. Daoud-Aladine *et al.*, Phys. Rev. Lett. **89**, 097205 (2002).
[11] S. Grenier *et al.*, Phys. Rev. B **69**, 134419 (2004).
[12] T. G. Perring *et al.*, Phys. Rev. Lett. **77**, 711 (1996).
[13] H. Y. Hwang *et al.*, Phys. Rev. Lett. **80**, 1316 (1998).
[14] J. W. Lynn *et al.*, Phys. Rev. Lett. **76**, 4046 (1996).
[15] Y. Endoh *et al.*, Phys. Rev. Lett. **94**, 017206 (2005).
[16] Y. Moritomo *et al.*, Phys. Rev. B **51**, 3297 (1995).
[17] S. Larochelle *et al.*, Phys. Rev. B **71**, 024435 (2005).
[18] D. Senff *et al.*, Phys. Rev. B **71**, 024425 (2005).
[19] B. J. Sternlieb *et al.*, Phys. Rev. Lett. **76**, 2169 (1996).
[20] P. Mahadevan *et al.*, Phys. Rev. Lett. **87**, 066404 (2001).
[21] S. Larochelle *et al.*, Phys. Rev. Lett. **87**, 095502 (2001).
[22] S. B. Wilkins *et al.*, Phys. Rev. Lett. **91**, 167205 (2003).
[23] S. S. Dhesi *et al.*, Phys. Rev. Lett. **92**, 056403 (2004).
[24] M. Tokunaga *et al.*, Phys. Rev. B **59**, 11 151 (1999).
[25] P. Reutler *et al.*, J. Cryst. Growth **249**, 222 (2003).
[26] D. Senff *et al.* (unpublished).
[27] F. Krüger and S. Scheidl, Phys. Rev. B **67**, 134512 (2003).
[28] F. Moussa *et al.*, Phys. Rev. B **54**, 15 149 (1996).
[29] N. Furukawa, J. Phys. Soc. Jpn. **65**, 1174 (1996).
[30] J. van den Brink *et al.*, Phys. Rev. Lett. **83**, 5118 (1999).
[31] D. V. Efremov *et al.*, Nat. Mater. **3**, 853 (2004).